Draft version November 26, 2015
Preprint typeset using LaTeX style emulateapj v. 12/16/11

COLLISIONS KILL KAPPA: ELECTRONS ARE ALWAYS MAXWELLIAN IN PHOTOIONIZED NEBULAE

W. J. Henney, G. J. Ferland, C. R. O'Dell, M. Peimbert

Draft version November 26, 2015

ABSTRACT

Non-Maxwellian electron speed distributions have recently been suggested as a novel solution to long-standing discrepancies in the interpretation of emission line ratios from photoionized gas in H II regions and planetary nebulae. The power-law tailed κ distribution has been proposed as an alternative to temperature or abundance fluctuations as a means of reconciling the relative strengths of collisionally excited and recombination lines of the same ion. We show that the plasma in photoionized regions is so overwhelmingly collisional (Knudsen number Kn = 10^{-10} to 10^{-6}) that deviations from a Maxwellian electron distribution have a negligible effect on diagnostic line ratios when integrated over an entire ionization-bounded nebula. This is true both for deviations induced by the photoionization/recombination process itself (including the case of a very hard ionizing continuum) and for any plausible scenario involving high-energy electrons (for example, cooling zones behind photoionized shocks, diffusion of electrons from a hot shocked stellar wind bubble, Auger ionization by x-rays, or magnetic reconnection). In all these scenarios, the observational effects of the resultant temperature fluctuations far exceed those of the tiny deviations from Maxwellian.

1. INTRODUCTION

Deviations from a Maxwellian electron velocity distribution in a plasma arise when significant non-local transport of electrons occurs, which is important if there are steep gradients in physical conditions (such as temperature). The dimensionless Knudsen number, Kn = λ/L, which describes the "collisionality" of the plasma, is the most important parameter in determining the importance of these deviations. This is the ratio between the electron elastic collisional mean free path, λ, and the relevant length scale, L, which is the distance over which physical conditions change appreciably (for instance, the scale length of the temperature gradient: $[d \ln T/ds]^{-1}$)

If Kn $\geq$ 1, then the plasma is "non-collisional" and the electron velocity distribution will be very different from a Maxwellian, and also non-isotropic in the presence of a significant magnetic field. An extreme example is the terrestrial magnetosphere, where Kn $\gg$ 1.

If Kn $<$ 1, then the plasma is "collisional" and as Kn $\to$ 0 the electron velocity distribution will tend towards a Maxwellian distribution at the local temperature. However, the fact that λ increases with electron velocity means that a significant high-energy non-Maxwellian tail can persist, even for rather small values of Kn. Quantities that are sensitive to this tail, such as thermal conductivity or the collisional excitation of optical/UV emission lines, can significantly deviate from the Maxwellian values for Kn as low as 0.001.

Theoretical explanations for the existence of kappa distributions as stationary equilibrium solutions to the Boltzmann equation have been found both for highly non-collisional (Kn > 1) plasmas (Pierrard & Lazar 2010; Livadiotis & McComas 2013) and for mildly collisional (Kn $\sim$ 0.01) plasmas in the presence of stochastic turbulent electron acceleration (Bian et al. 2014).

In H II regions, Kn $\approx 1 \times 10^{-9}$ for the region as a whole, but certain sub-structures can have smaller values:

- Ionization fronts (where hydrogen rapidly changes from being prefominantly ionized to predominantly neutral) have Kn $\simeq 1 \times 10^{-6}$.
- Cooling zones behind moderate velocity (20–100 km s^{-1}) shocks also have Kn $\simeq 1 \times 10^{-6}$.

However, the emission from the both ionization fronts and post-shock cooling zones is typically only a tiny fraction of the total emission from the region (unless the ionization parameter is very low).

2. SUPRATHERMAL ELECTRONS IN SOLAR PHYSICS AND GEOPHYSICS

Summary of observations and modeling of the Transition Region, Coronal Loops, Solar Wind, and Terrestrial Magnetosphere.

Red dots show empirically estimated values of κ for the solar wind acceleration zone (Esser & Edgar 2000) (red dots, with the value for the innermost region at Kn = $2e-3$ being a lower limit)

3. THE COLLISIONALITY OF H II REGIONS AND STRUCTURES WITHIN THEM

As described in the introduction, the collisionality of a plasma is described by the Knudsen number Kn = λ/L. The relevant mean free path λ is the "deflection distance", which is the distance over which an electron's trajectory is deflected by 90° due to very many glancing Coulomb interactions with other charged particles (principally electrons and protons) in the plasma. For thermal electrons of temperature T_e and number density $n_e$this is given by

$$\lambda_0 = 2.625 \times 10^5 \frac{T_e^2}{n_e \ln \Lambda} \text{ cm} \qquad (1)$$

where the slowly varying Coulomb logarithm ($\ln \Lambda = 9.452 + 1.5 \ln T_e - 0.5 \ln n_e$ for $T_e < 4.2 \times 10^5$ K) accounts for the cut-off in electrostatic interactions beyond the Debye radius. For a typical H II region temperature of $T_e = 10^4$ K this becomes $\lambda_0 \simeq 1.3 \times 10^{12} n_e^{-1}$ cm. This value is appropriate for electrons with velocities close to the peak thermal velocity $\hat{u} = \sqrt{2kT_e/m_e} \simeq 550$ km s^{-1} and with energies of order 1 eV. The deflection mean free path is substantially longer for higher energy electrons, scaling with velocity as u^4 or with energy as E^2.

We first estimate the Knudsen number for an idealised homogeneous dust-free ionization-bounded H II region by taking the scale length L as being the Strömgren radius R_s =

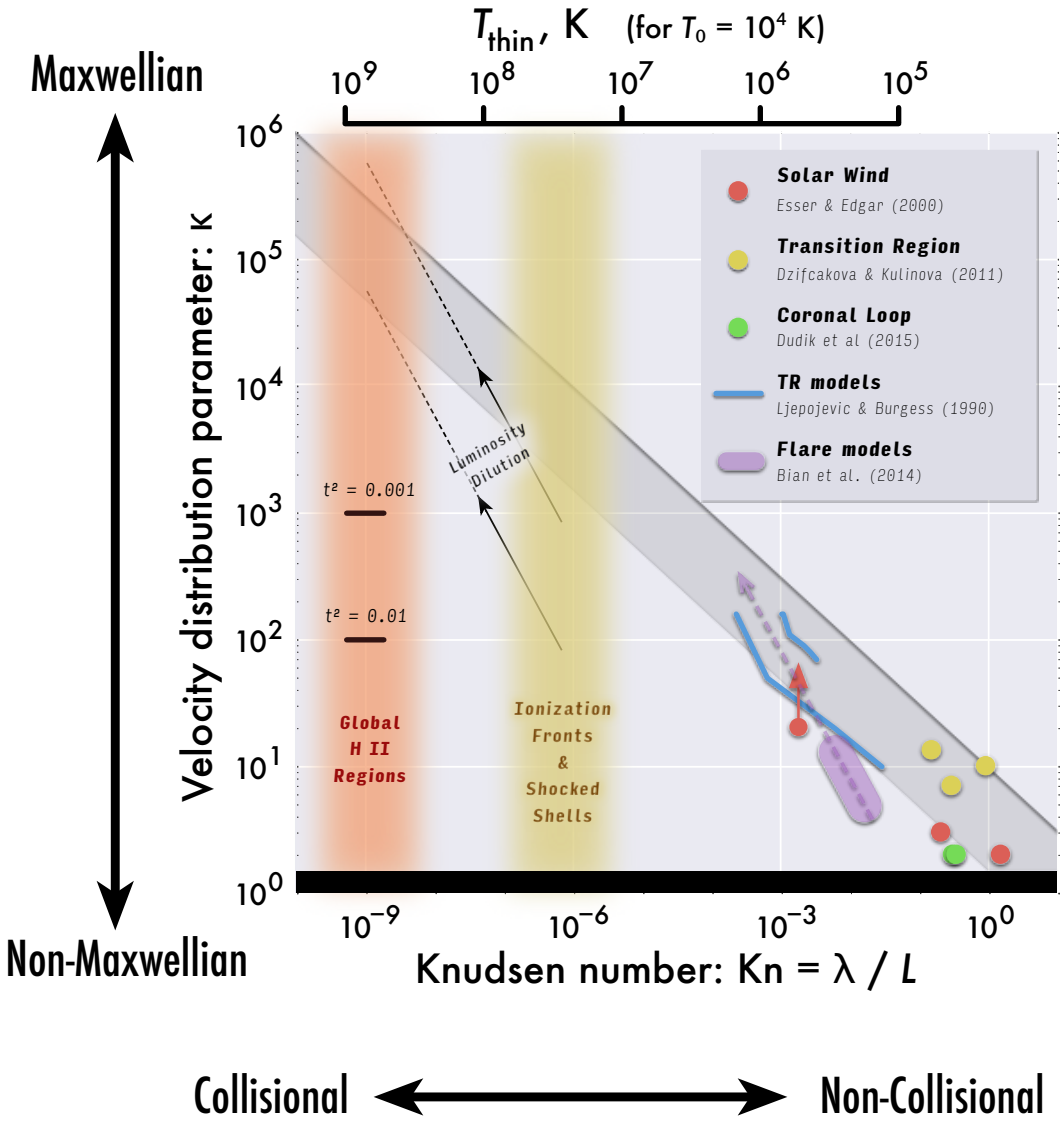

FIG. 1.— Location of H II regions and selected solar phenomena in the plane of Kappa (non-Maxwellian parameter) versus Knudsen number (plasma collisionality parameter). Colored dots show empirically estimated values of κ for the solar wind acceleration zone, the transition region between the chromosphere and corona, and for a coronal loop (see text for details). Colored lines show theoretical results from modelling non-local electron transport downwards through the transition region, and stochastic electron acceleration in solar flares (again, explained in more detail in the text). The diagonal darker gray band shows the relationship $\kappa \sim \mathrm{Kn}^{-1/2}$, which has no theoretical basis but which roughly captures the empirical trend seen in solar studies. H II regions and smaller-scale structures within them are represented by a fuzzy vertical bands to the left of the figure. The auxiliary horizontal scale at the top of the graph shows the temperature above which thermal electrons can freely stream along magnetic field lines over a length scale of order the size of the region (assuming background ionized gas at 10^4 K.)

TABLE 1
PHYSICAL CONDITIONS IN DIFFERENT CLASSES OF PHOTOIONIZED NEBULAE

Class	Example	Q_{49}	n	U
OB runaway nebula	ζ Oph/Sh 2-27	0.04	3	0.0003
Old planetary nebula	Helix Nebula	0.01	100	0.0006
Spitzer "Bubble"	RCW 120	0.3	1000	0.004
Compact H II region	Orion Nebula	1.0	10^4	0.02
Giant H II region	Carina, 30 Doradus	100	100	0.02
Super star cluster	Arches, M82 SSCs	1000	10^6	0.6
AGN Broad line regions				~ 0.1

$(3Q_H/4\pi\alpha_B n^2)^{1/3}$, where $n \simeq n_e$ is the ionized hydrogen density, Q_H is the rate of ionizing photons ($h\nu > 13.6$ eV) emitted by the source, and $\alpha_B \simeq 2.6 \times 10^{-13}$ cm^3 s^{-1} is the Case B hydrogen recombination coefficient. We also introduce the global dimensionless ionization parameter $U = Q_H/4\pi R_s^2 nc$, where c is the speed of light, which is roughly an average ratio between the ionizing photon density and particle density in the nebula. We thus find $R_s = 3.46 \times 10^{23} U n^{-1}$ cm, from which it follows that the Strömgren Knudsen number is

$$\mathrm{Kn}_s = 3.76 \times 10^{-12} U^{-1},$$

which depends only on the ionization parameter and not on the density. It also follows from the above equations that the ionization parameter is $U \simeq 6 \times 10^{-4} (Q_{49} n)^{1/3}$, where Q_{49} is the ionizing luminosity normalized to 10^{49} s^{-1}, which is a typical value for a single O-type star. Values of Q_{49}, n, and U for different types of ionized nebulae are shown in Table 1.

vary from $U \simeq 0.0006$ for an evolved planetary nebula ($Q_{49} \simeq 0.01$, $n \simeq 100$ cm^{-3}) up to $U \simeq 0.02$ for a compact H II region ($Q_{49} \simeq 1$, $n \simeq 10^4$ cm^{-3}), implying $\mathrm{Kn}_s \approx 10^{-10}$–$10^{-8}$.

Super star clusters in M82 (McCrady & Graham 2007; Krumholz & Matzner 2009). OB runaway nebula (Gvaramadze et al. 2012). Spitzer bubble (Deharveng et al. 2009). Carina (Smith & Brooks 2008) 30 Dorados (Torres-Flores et al. 2013)

Do we want to mention case of photoevaporation flows

Look at AGN. BLR (Baskin et al. 2014), NLR (Dopita et al. 2002; Groves et al. 2004)

Quasar environments can have $U > 1$ and very hard ionizing spectra, in which case Compton heating becomes important and the equilibrium T_e becomes an increasing function of U, potentially reaching $> 10^5$ K Sazonov et al. (2004). *We don't want to go there.*

4. EQUILIBRIUM ELECTRON DISTRIBUTIONS IN PHOTOIONIZED PLASMAS

In a steady state homogeneous photoionized plasma, in the absence of external macroscopic forces, the electron velocity distribution function f_u will satisfy the equation:

$$\left(\frac{\partial f_u}{\partial t}\right)_{\mathrm{elastic}} + \left(\frac{\partial f_u}{\partial t}\right)_{\mathrm{photo}} + \left(\frac{\partial f_u}{\partial t}\right)_{\mathrm{recomb}} + \left(\frac{\partial f_u}{\partial t}\right)_{\mathrm{inelastic}} = 0, \quad (2)$$

where the four terms on the left hand side represent respectively elastic collisions, photoionization, recombination, and inelastic collisions. Note that the distribution function is normalized to $\int_0^\infty f_u \, du = 1$. We now consider each individual term in detail.

Elastic collisions— $(\partial f_u/\partial t)_{\mathrm{elastic}}$ is the traditional collisional redistribution integral in the Boltzmann equation (e.g., Pitaevskii & Lifshitz 1981), also known as the Fokker–Planck operator, which tends to drive the velocity distribution towards thermal equilibrium. A rigorous treatment of this term is difficult and we instead adopt the BGK approximation, first introduced by Bhatnagar et al. (1954), in which the collision integral is replaced by a simple relaxation toward a Maxwellian distribution f_u^*:

$$\left(\frac{\partial f_u}{\partial t}\right)_{\mathrm{elastic}} = -\frac{1}{\tau}(f_u - f_u^*), \quad (3)$$

where $\tau = \lambda/u$ is the elastic collisional timescale. This is a source term ($(\partial f_u/\partial t)_{\mathrm{elastic}} > 0$) at velocities where the distribution is sub-Maxwellian ($f_u < f_u^*$) and is a sink term ($(\partial f_u/\partial t)_{\mathrm{elastic}} < 0$) at velocities where the distribution is supra-Maxwellian ($f_u > f_u^*$). Thus, acting alone, $(\partial f_u/\partial t)_{\mathrm{elastic}}$ would drive the electrons to a Maxwellian distribution, $f_u \to f_u^*$, on a timescale τ.

Since the BGK approximation is only phenomenological, different possible choices exist for the exact form of the relaxation timescale τ (see § 5.3 of Spitzer 1956). Livi & Marsch (1986) compared the BGK approximation with evaluation of the full Fokker-Planck operator when calculating the time-dependent relaxation of initially anisotropic bi-Maxwellian and double-beam configurations. They found that the closest correspondence was obtained by using the velocity-space friction timescale τ_F. If ξ is the electron velocity expressed in units of the most probable thermal speed ($\xi = u/\hat{u}$) then

$$\tau_F = \frac{\tau_0 \, \xi^2}{\mathrm{erf}\, \xi - \xi \, \mathrm{erf}'\xi}, \quad (4)$$

where $\tau_0 = \lambda_0/\hat{u}$, with λ_0 given by equation (1), and erf, erf′ are respectively the error function and its derivative. Other possible choices are the slowing down timescale

$$\tau_s = \xi \tau_F \quad (5)$$

and the deflection timescale

$$\tau_d = \frac{2\tau_0 \, \xi^5}{(2\xi^2 - 1)\,\mathrm{erf}\, \xi + \xi \, \mathrm{erf}'\xi}. \quad (6)$$

All three are shown in Figure 2, where it is apparent that only τ_F diverges both for very small and very large velocities, meaning that elastic collisions take longer to Maxwellianize the low-energy and high-energy tails of the distribution. The other two timescales increase monotonically with u, meaning that the low velocity electrons will Maxwellianize most rapidly. Below, we investigate the effects of using each of these timescales in the relaxation operator.

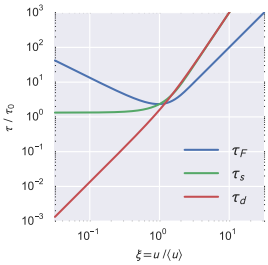

	$u \ll \hat{u}$	$u \gg \hat{u}$
τ_F	$\propto u^{-1}$	$\propto u^2$
τ_s	constant	$\propto u^3$
τ_d	$\propto u^2$	$\propto u^3$

FIG. 2.— Three different candidate relaxation timescales as a function of electron velocity in thermal units. Velocity-space friction timescale τ_F (blue line), slowing down time τ_s (green line), and deflection time τ_d (red line). Asymptotic behaviors for small and large velocities are shown in the table.

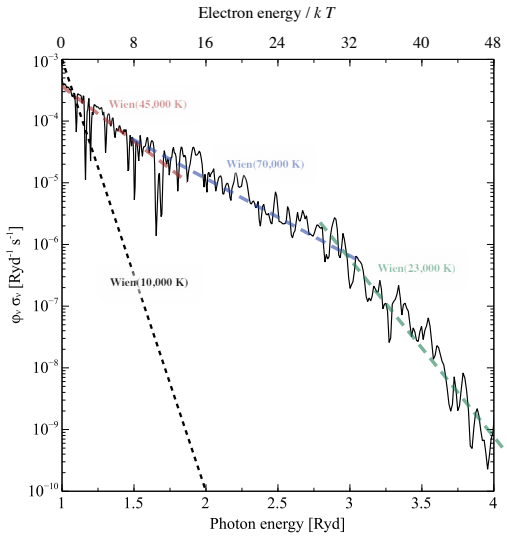

FIG. 3.— Semilogarithmic plot of photoelectric yield as a function of ionizing photon energy (lower horizontal scale) or photoelectron energy (upper horizontal scale) from a Cloudy model of the Orion Nebula. Dashed colored lines show approximate piecewise Wien (exponential) fits to the data. Dashed black line shows high energy tail of 10,000 K Maxwellian distribution.

Photoionizations — $(\partial f_u/\partial t)_{\rm photo}$ represents the rate of production of photo-electrons with velocity u due to the photoionization of neutral hydrogen or atoms/ions of other elements. Consider the photoionization of H from the ground level (see § 2.2 of Osterbrock & Ferland 2006) by photons of energy $h\nu$. The resultant photo-electron will have energy $\frac{1}{2}m_e u^2 = h\nu - h\nu_0$, where $h\nu_0 = 13.6$ eV is the H ionization potential. The ionizing photon intensity is represented by

$$\phi_\nu = \frac{4\pi J_\nu}{h\nu} \text{ photons s}^{-1} \text{ cm}^{-2} \text{ Hz}^{-1}, \qquad (7)$$

where J_ν is the mean intensity of the radiation field. If $n(\mathrm{H}^0)$ is the number density of neutral H, and a_ν is the frequency-dependent photoionization cross-section (approximately proportional to ν^{-3} for $\nu > \nu_0$), then the photo-electron production rate per unit volume and per unit velocity interval is

$$n_e\left(\frac{\partial f_u}{\partial t}\right)_{\rm photo} = n(\mathrm{H}^0)\phi_\nu a_\nu \frac{d\nu}{du}. \qquad (8)$$

Similar contributions will arise from the ionization of neutral helium, singly ionized helium, and heavier elements. Figure 3 shows the product $\phi_\nu a_\nu$ (except in energy rather than frequency units) at the illuminated face of a Cloudy model of the Orion Nebula, with the ionizing spectrum calculated from stellar atmosphere models (Lanz & Hubeny 2003) of the 5 OB stars of the Trapezium cluster (Ferland et al. 2012). *Does this include dust photoionization? Does it include the OTS diffuse field?*. The photoelectric yield can be approximately fit by piecewise exponential Wien functions, $\exp(-E/kT_*)$, as shown on the figure. For photon energies between the H^0 and He^0 ionization edges (1 to 1.8 Rydbergs, corresponding to photoelectron energies $\lesssim 10kT_e$), we find $T_* \simeq 45{,}000$ K. This is close to the effective temperature of the most luminous ionizing star, and much larger than the equilibrium electron temperature in the H II region, meaning that the high-energy tail of f_u will be preferentially populated by this mechanism.

Recombinations — $(\partial f_u/\partial t)_{\rm recomb}$ represents the rate of loss of electrons due to radiative recombination with protons and other ions. For recombinations to all excited ($n > 1$) bound states nL of hydrogen, the electron loss rate per unit volume and unit velocity interval is (e.g., § 4.3 of Ferland et al. 2012)

$$n_e\left(\frac{\partial f_u}{\partial t}\right)_{\rm recomb} = -n_e n_p u f_u \sum_{n=2}^{\infty}\sum_{L=0}^{n-1} \sigma(\mathrm{H}^0_{nL}, u), \qquad (9)$$

where $\sigma(\mathrm{H}^0_{nL}, u)$ are the radiative recombination cross-sections, which can be expressed in terms of the photoionization cross-sections as

$$\sigma(\mathrm{H}^0_{nL}, u) = (2L+1)\frac{h^2\nu^2}{m_e^2 c^2 u^2} a_\nu(\mathrm{H}^0_{nL}) \qquad (10)$$

in which $h\nu = \frac{1}{2}m_e u^2 + h\nu_0/n^2$. *Do we just ignore the recombinations to the ground state? Does Cloudy have a way of simply printing out these terms. We could perhaps calculate them from the free-bound continuum spectra.*

Inelastic collisions — $(\partial f_u/\partial t)_{\rm inelastic}$ represents both a source of lower velocity electrons and also a sink of higher velocity electrons due to the collisional excitation of bound-bound transitions in atoms and ions, followed by their spontaneous radiative decay. It is only important for transitions with critical densities $n_{\rm crit} \gtrsim n_e$ since super-elastic collisional de-excitations are in equilibrium with inelastic collisional excitations in the limit $n_{\rm crit} \ll n_e$, leading to zero net contribution to $(\partial f_u/\partial t)_{\rm inelastic}$.

The net production rate per unit volume and unit velocity interval of electrons with velocity u due to collisional excitation of an ion from level 1 to level 2 with energy difference χ_{12} is

$$n_e\left(\frac{\partial f_u}{\partial t}\right)_{\rm inelastic} = n_e n_1\left[u'\sigma_{12}(u')f_{u'} - u\sigma_{12}(u)f_u\right], \qquad (11)$$

where $u' = (u^2 + 2\chi_{12}/m_e)^{1/2}$ and n_1 is the density of ions in level 1. The collisional cross section is

$$\sigma_{12}(u) = \frac{\pi\hbar^2}{m_e^2 u^2}\frac{\Omega_{12}(u)}{\omega_1} \quad \text{for} \quad \tfrac{1}{2}mu^2 \geq \chi_{12} \qquad (12)$$

where ω_1 is the statistical weight of level 1 and $\Omega_{12}(u)$ is the velocity-dependent collision stremgth.

As an example, we consider the ${}^3P_{0,1,2}{-}{}^1D_2$ and ${}^3P_{0,1,2}{-}{}^1S_0$ transitions in [O III], which give rise at optical wavelengths to emission of the strong λ5007, λ4959 nebular lines, and the weaker λ4363 auroral line. Results are shown in Figure 4, where the transfer of electrons from the high-velocity side to the low-velocity side of the distribution is apparent. Thus, inelastic collisions act in opposition to the photoionization-recombination process, which transfers electrons in the other direction. This is a direct manifestation of the competition between photo-heating and collisional line cooling that determines the thermal balance in photoionized gas.

Electrons with energies greater than 0.75 Rydberg ($\xi \gtrsim 3.5$) can collisionally excite the H^0 Lyman lines. At nebular temperatures this is not an important cooling mechanism because the Maxwellian population of such high energy electrons is so small: $f_u \sim e^{-\xi^2} \approx 10^{-5}$. However, for the few electrons that *do* have such high energies it will be an important sink term. Similarly, electrons more energetic than 1 Rydberg can collisionally ionize H^0, which can also be considered as a kind of inelastic collision in which a high energy electron is converted

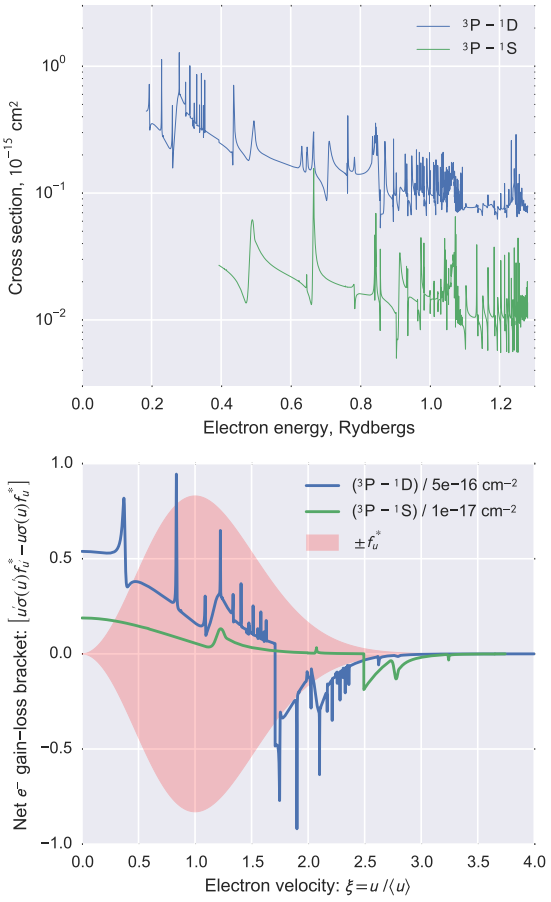

FIG. 4.— *Upper panel*: Collisional excitation cross sections from the ground term of [O III] to the excited levels responsible for the optical nebular and auroral lines. The cross sections are calculated using energy-dependent collision strengths from Storey et al. (2014) and correspond to the sum of the excitations from the three fine-structure levels of the ground term, $^3P_0$, $^3P_1$, and $^3P_2$. Each ^3P level is assumed to be populated in proportion to its statistical weight, which is appropriate for electron densities higher than the critical densities of 3600 cm^{-3} for $^3P_2$ and 510 cm^{-3} for $^3P_1$. *Lower panel*: Net bracketed term from equation (11) for the same two [O III] transitions, assuming a Maxwellian electron speed distribution, $f_u = f_u^*(10,000\ \mathrm{K})$, shown in red. Inelastic collisions act to depopulate the high-velocity tail of the distribution where the bracket is negative ($u > 1.7\hat{u}$ for $^1D_2$ and $u > 2.5\hat{u}$ for $^1S_0$). At the same time they repopulate the core and low-velocity tail of the distribution where the bracket is positive.

into two lower energy electrons with velocities u' and u'' that satisfy

$$\frac{1}{2}m_e u^2 = h\nu_0 + \frac{1}{2}m_e u'^2 + \frac{1}{2}m_e u''^2. \qquad (13)$$

5. DIFFUSION OF HIGH ENERGY ELECTRONS THROUGH PHOTOIONIZED GAS

5.1. *Cooling zone behind low-velocity shocks*

Spitzer–Härm approximation is valid for $\xi < \xi_c = \mathrm{Kn}_T^{-1/4}$ (Shoub 1983), where the temperature-gradient Knudsen number is $\mathrm{Kn}_T = \lambda_0 d\ln T/dz$. So, with Kn = 0.0065 which I get from the shock models, we find $\xi_c = 3.5$. Thus, for $\xi < 3.5$ we have

$$f_u(\xi,\mu,z) = f_u^*(\xi,z)\Big[1 + \mu\,\mathrm{Kn}\,D(\xi) + O(\mathrm{Kn}^2)\Big] \qquad (14)$$

where $D(\xi)$ is given in Table II of Spitzer & Härm (1953). This implies that the deviation of the angle-averaged distribution function from Maxwellian is of order $(\mathrm{Kn})^2$ for $\xi < \xi_c$.

We should check this against results of BGK calculations.

5.2. *Leakage of hot electrons from stellar wind bubbles*

Recent models of stellar wind bubbles inside H II regions (Mackey et al. 2015)

Survey of H II regions in LMC and SMC (Lopez et al. 2014) give X-ray emitting hot gas with $T = 2$–8×10^6 K and density 0.01–0.3 cm^{-3}. *Also look at* ... Carina (Townsley et al. 2011)

Need to consider inelastic interactions that would effect the hot electrons, such as collisional ionization. But according to §11.3.3 of Osterbrock & Ferland (2006) this is only important for ionization fractions less than 0.9 (should it be 0.1?). This is treated in more detail in Furlanetto & Stoever (2010) who carry out Monte Carlo simulations of electrons from 10 eV to 10 keV, albeit for primordial abundances, finding that heating is completely dominant when the gas is more than a little bit ionized. For instance, with ionization fraction of 0.9–0.999 and 3 keV electrons, 98% of energy goes into heating through elastic collisions and 2% goes into ionization, nearly all of which is of He.

They have an interesting way of treating the energy loss in the elastic collisions by discretization. Assume an arbitrary fixed fraction f of energy is lost in individual "collision" events, for which one can work out an effective cross-section, which will be $\propto 1/f$. They cite Habing & Israel (1979) and Shull (1979) for this. Perhaps we could adapt it to our case, but we need to take a quite small $f \sim 10^{-4}$ so that the energy given to the thermal electrons in each "interaction" is a fraction of an eV.

In Spitzer & Scott (1969) it is argued that the dispersion in energies of initially monoenergetic non-thermal electrons is small as they lose energy by elastic collisions. The quote is

> *Hence, if a group of secondary electrons all have the same energy initially, their dispersion of energies after one energy-loss time will be small compared with their initial energy.*

It seems that the energy loss of the non-thermal electrons does not occur via a "cascade" as I had originally supposed, but rather is a gradual slowing down of the high-velocity electron, with the energy going in to general heating of the thermal electrons. If this is true, then it makes the BGK approximation much more defensible, even for this case.

Also include Auger electrons from inner shell photoionization by X-rays as a source of high energy electrons. Compared with those that come from stellar wind bubble these have the advantage that they are created throughout the nebula.

Dust contribution from Weingartner et al. (2006)

*General argument about why keV electrons will never, **ever** affect the excitation of an auroral line like 4363 unless they actually raise the temperature of the gas.* — The electrons start with energy E that is 1000 times that of thermal electrons ($\xi \approx 30$). They lose energy on a timescale τ_E that is u^3 or $E^{3/2} = 3 \times 10^4$ times longer than the elastic collisional timescale τ_0 of the thermal electrons. The auroral lines are sensitive to the electrons in the tail of the thermal distribution with $\xi \approx 2.5$–3.5. In order for the keV electrons to lose 99% of their energy so as to get down to such thermal tail speeds will take about $\tau_{99} = \log_e(100) \times \tau_E \approx 10^5\tau_0 \approx 100\,n_e^{-1}$ years. During that time, the energy is transferred to the thermal gas via "friction", thus raising its temperature slightly. *(Is there a simple way of estimating*

how this is shared out as a function of ξ?) The energy is not yet radiated away because the radiative cooling timescale of the thermal gas is much longer at $t_{\rm cool} \approx 2 \times 10^4 n_e^{-1}$ years. The relaxation time of the $\xi \sim 3$ thermal tail electrons is $\tau_{\rm tail} \approx 30\tau_0 \approx 0.02$ years, so they remain Maxwellian at the new temperature.

Suppose that high energy electrons (with speeds $\xi_h \approx 30$) are impulsively injected into a photoionized region at $t = 0$. Suppose that the initial energy density of the high energy electrons is a fraction $\delta \ll 1$ times the energy density $\frac{3}{2}kT$ of the thermal gas. Therefore the initial amplitude of the distribution function at $\xi = \xi_h$ is $f_h \approx \delta/\xi_h$. By a time $t = \tau_{99}$ they have slowed down to $\xi = \xi_t \simeq 3$, but their amplitude remains the same. At the same time, the temperature of the thermal gas has been raised to $T' = (1+\delta)T$. This will increase the thermal tail population from $\exp(-\xi_t^2)$ to $\exp(-\xi_t^2/(1+\delta))$.

Show this graphically – it will be much clearer

5.3. *Effects of magnetic fields*

Diffusion across field lines is greatly suppressed. *But look into Bohm diffusion (only 2D case?) and Hsu diffusion (3D), which give perpendicular transport coefficients much larger than the classical values.*

REFERENCES

Baskin, A., Laor, A., & Stern, J. 2014, MNRAS, 438, 604
Bhatnagar, P. L., Gross, E. P., & Krook, M. 1954, Physical Review, 94, 511
Bian, N. H., Emslie, A. G., Stackhouse, D. J., & Kontar, E. P. 2014, ApJ, 796, 142
Deharveng, L., Zavagno, A., Schuller, F., Caplan, J., Pomarès, M., & De Breuck, C. 2009, A&A, 496, 177
Dopita, M. A., Groves, B. A., Sutherland, R. S., Binette, L., & Cecil, G. 2002, ApJ, 572, 753
Esser, R., & Edgar, R. J. 2000, ApJ, 532, L71
Ferland, G. J., Henney, W. J., O'Dell, C. R., Porter, R. L., van Hoof, P. A. M., & Williams, R. J. R. 2012, ApJ, 757, 79
Furlanetto, S. R., & Stoever, S. J. 2010, MNRAS, 404, 1869
Groves, B. A., Dopita, M. A., & Sutherland, R. S. 2004, ApJS, 153, 9
Gvaramadze, V. V., Langer, N., & Mackey, J. 2012, MNRAS, 427, L50
Habing, H. J., & Israel, F. P. 1979, ARA&A, 17, 345
Krumholz, M. R., & Matzner, C. D. 2009, ApJ, 703, 1352
Lanz, T., & Hubeny, I. 2003, ApJS, 146, 417
Livadiotis, G., & McComas, D. J. 2013, Space Sci. Rev., 175, 183
Livi, S., & Marsch, E. 1986, Phys. Rev. A, 34, 533
Lopez, L. A., Krumholz, M. R., Bolatto, A. D., Prochaska, J. X., Ramirez-Ruiz, E., & Castro, D. 2014, ApJ, 795, 121
Mackey, J., Gvaramadze, V. V., Mohamed, S., & Langer, N. 2015, A&A, 573, A10
McCrady, N., & Graham, J. R. 2007, ApJ, 663, 844
Osterbrock, D. E., & Ferland, G. J. 2006, Astrophysics of gaseous nebulae and active galactic nuclei, 2nd edn. (Sausalito, CA: University Science Books)
Pierrard, V., & Lazar, M. 2010, Sol. Phys., 267, 153
Pitaevskii, L., & Lifshitz, E. 1981, Course of Theoretical Physics, Vol. 10, Physical Kinetics, ed. L. Landau & E. Lifshitz (Pergamon Press)
Sazonov, S. Y., Ostriker, J. P., & Sunyaev, R. A. 2004, MNRAS, 347, 144
Shoub, E. C. 1983, ApJ, 266, 339
Shull, J. M. 1979, ApJ, 234, 761
Smith, N., & Brooks, K. J. 2008, The Carina Nebula: A Laboratory for Feedback and Triggered Star Formation, ed. B. Reipurth, 138–+
Spitzer, L. 1956, Physics of Fully Ionized Gases
Spitzer, L., & Härm, R. 1953, Physical Review, 89, 977
Spitzer, Jr., L., & Scott, E. H. 1969, ApJ, 158, 161
Storey, P. J., Sochi, T., & Badnell, N. R. 2014, MNRAS, 441, 3028
Torres-Flores, S., Barbá, R., Maíz Apellániz, J., Rubio, M., Bosch, G., Hénault-Brunet, V., & Evans, C. J. 2013, ArXiv e-prints
Townsley, L. K., Broos, P. S., Chu, Y.-H., Gruendl, R. A., Oey, M. S., & Pittard, J. M. 2011, ApJS, 194, 16
Weingartner, J. C., Draine, B. T., & Barr, D. K. 2006, ApJ, 645, 1188